HHS Public Access

Author manuscript

Stem Cells. Author manuscript; available in PMC 2015 March 10.

Published in final edited form as:

Stem Cells. 2011 August ; 29(8): 1241–1255. doi:10.1002/stem.670.

Dura Mater Stimulates Human Adipose-Derived Stromal Cells to Undergo Bone Formation in Mouse Calvarial Defects

Benjamin Levi[a], **Emily R. Nelson**[a], **Shuli Li**[a], **Aaron W. James**[a], **Jeong S. Hyun**[a], **Daniel T. Montoro**[a], **Min Lee**[b], **Jason P. Glotzbach**[a], **George W. Commons**[a], and **Michael T. Longaker**[a,c]

[a]Hagey Laboratory for Pediatric Regenerative Medicine, Plastic and Reconstructive Surgery Division, Department of Surgery, Stanford University School of Medicine, Stanford, California, USA

[b]Division of Advanced Prosthodontics, Biomaterials, and Hospital Dentistry, University of California, Los Angeles, School of Dentistry, Los Angeles, California, USA

[c]Institute for Stem Cell Biology and Regenerative Medicine, Stanford University, Stanford, California, USA

Abstract

Human adipose-derived stromal cells (hASCs) have a proven capacity to aid in osseous repair of calvarial defects. However, the bone defect microenvironment necessary for osseous healing is not fully understood. In this study, we postulated that the cell-cell interaction between engrafted ASCs and host dura mater (DM) cells is critical for the healing of calvarial defects. hASCs were engrafted into critical sized calvarial mouse defects. The DM-hASC interaction was manipulated surgically by DM removal or by insertion of a semipermeable or nonpermeable membrane between DM and hASCs. Radiographic, histologic, and gene expression analyses were performed. Next, the hASC-DM interaction is assessed by conditioned media (CM) and coculture assays. Finally, bone morphogenetic protein (BMP) signaling from DM was investigated in vivo using novel BMP-2 and anti-BMP-2/4 slow releasing scaffolds. With intact DM, osseous healing occurs both from host DM and engrafted hASCs. Interference with the DM-hASC interaction dramatically reduced calvarial healing with abrogated BMP-2–Smad-1/5 signaling. Using CM and coculture assays, mouse DM cells stimulated hASC osteogenesis via BMP signaling. Through in vivo manipulation of the BMP-2 pathway, we found that BMP-2 plays an important role in DM

Correspondence: Michael T. Longaker, M.D., M.B.A., Hagey Laboratory for Pediatric Regenerative Medicine, Stanford University School of Medicine, 257 Campus Drive, Stanford University, Stanford, California 94305-5148, USA. Telephone: 650-736-1707; Fax: 650-736-1705; Longaker@stanford.edu.

Author contributions: B.L.: conception and design, administrative support, collection and/or assembly of data, data analysis and interpretation, manuscript writing; E.R.N.: administrative support, collection and/or assembly of data, data analysis and interpretation, manuscript writing; S.L. and J.S.H.: collection and/or assembly of data, data analysis and interpretation; A.W.J.: collection and/or assembly of data, data analysis and interpretation, manuscript writing; D.T.M.: collection and/or assembly of data; M.L. and G.W.C.: provision of study material or patients; J.P.G.: collection and assembly of data; M.T.L.: conception and design, final approval of manuscript.

Disclosure of Potential Conflicts of Interest

The authors indicate no potential conflicts of interest. University of Stanford IRB approval was obtained before commencement of the study (IRB# 2188, 9999).

stimulation of hASC osteogenesis in the context of calvarial bone healing. BMP-2 supplementation to a defect with disrupted DM allowed for bone formation in a nonhealing defect. DM is an osteogenic cell type that both participates in and stimulates osseous healing in a hASC-engrafted calvarial defect. Furthermore, DM-derived BMP-2 paracrine stimulation appears to play a key role for hASC mediated repair.

Keywords

Skeletal tissue engineering; Tissue regeneration; Multipotent stromal cells; Calvarial defect; Dura mater; Bone morphogenetic protein

Introduction

Calvarial skeletal regeneration requires a dynamic balance between osteoblasts, periosteal cells, and underlying dura mater (DM) cells. Children younger than 18–24 months have the remarkable capacity to regenerate bone from large calvarial defects. However, this capability is largely lost after 2 years of age [1, 2]. Similarly, numerous animal studies have demonstrated a difference in calvarial reossification between juveniles and adults [1, 3–6]. Loss of regenerative capacity in adults has been linked to differences in the underlying DM between juvenile and adult animals [7, 8]. For example, studies have demonstrated that transplantation of DM from a juvenile rat to an adult rat allowed for calvarial healing [9]. Furthermore, our laboratory has demonstrated that the DM and regenerating bone in a juvenile defect express significantly greater amounts of bone morphogenetic protein-2 (BMP-2), BMP-4, and BMP-7 [10]. If adult DM is insufficient to stimulate healing of calvarial defects, cell and cytokine-based therapies become necessary to allow osseous healing in adults.

One such suitable multipotent stem cell source for skeletal tissue engineering efforts is adipose-derived stromal cells (ASCs). Recent clinical studies have focused on the use of human ASCs (hASCs) to heal osseous defects [11–17]. Such reconstructions deliver a population of cells that can undergo osteogenic differentiation and eliminate the need for alloplastic materials. In this study, we examined the role of the underlying DM and implanted hASCs on bone repair, using a nude mouse calvarial defect model.

Despite accumulating translational research, there is a paucity of data defining the mechanisms through which hASCs interact with surrounding tissues in an osseous defect. In the case of calvarial defects, careful examination of radio-graphic and histologic data suggests that the underlying DM may play a role in the ossification of hASC-engrafted defects. For example, small, isolated islands of bone in the center of the defect are often observed early postoperatively, rather than peninsulas or areas of ossification contiguous to encircling intact host calvarial bone. In comparison, non-hASC-engrafted defects show a near complete absence of bone. These observations led us to hypothesize that the DM-hASC interaction may be a crucial one for hASC mediated bony repair. Cells derived from DM have been well-defined both as an osteocompetent cell source (able to differentiate toward an osteogenic lineage) and a potent source of pro-osteogenic cytokines [8, 18, 19]. In this

study, we postulated that the cell-cell interaction between engrafted ASCs and host DM cells is important for the healing of calvarial defects.

DM cells originates from a thin layer of neural crest-derived cells that migrate with the cerebral tissue [20, 21]. These neural crest cells have been shown to stimulate osteogenesis of the overlying bone tissues in a region-specific manner. Various signaling cascades have been identified including the fibroblast growth factor (FGF) and transforming growth factor (TGF)-β pathways [20]. Despite the known role of FGF secreted by DM on the overlying tissues, FGF-2 has been shown to have an inhibitory role on the osteogenic differentiation of ASCs [22]. Another pathway indicated in the osteogenic potential of DM is the BMP pathway, because BMP-2, BMP-4, and BMP-7 have been shown to be expressed in the DM [10]. BMPs are members of the TGF-β superfamily and initiates their signaling cascade through BMP receptor types I and II. These activated receptor kinases subsequently phosphorylate transcription factors SMAD-1, SMAD-5, and SMAD-8 [23]. These phosphorylated SMADs (pSMADs) form a heterodimeric complex with Smad-4 and stimulate target genes such as Msh homeobox-2 and Runt-related protein-2 (RUNX-2) [24–27]. This signaling cascade initiated by BMP-2 has been shown to induce significant osteogenesis in mesenchymal cells in vitro and has been used successfully in spinal reconstruction trials in vivo [28–32].

To examine the potential interaction between host DM cells and implanted hASCs, we set out to perform a series of in vivo and in vitro experiments. First, the osteogenic healing capacity of critical sized calvarial defects was analyzed either with the DM intact, removed, or blocked by a semipermeable or nonpermeable membrane. To further define this paracrine interaction, conditioned media (CM) and noncontact coculture experiments were performed with mouse DM cells and hASCs. These experiments suggested that BMP-2 signaling in the DM cells had an effect on the overlying hASCs. These studies culminated in using an anti-BMP-2/4 releasing scaffold to inhibit osseous healing of a defect with the DM intact, and more importantly, we demonstrate that a BMP-2 releasing scaffold can “rescue” defect healing in animals without DM—thus proving the importance of DM and DM-derived BMP-2 in hASC calvarial healing.

Materials and Methods

Chemicals, Supplies, and Animals

All mediums were purchased from GIBCO Life Technologies (Carlsbad, CA, www.lifetechnologies.com). Neutralizing BMP-2/4 antibody and recombinant human BMP-2 (rhBMP-2) were purchased from R&D Systems (Minneapolis, MN, http://www.rndsystems.com). CD-1 wild-type mice and CD-1 nude mice (Crl:CD-1 *Foxn1*^{nu}) were obtained from Charles River (Wilmington, MA, www.criver.com). Care of animals was in accordance with institutional guidelines.

Cell Harvest

hASCs were harvested from human lipoaspirates derived from six women with no major medical comorbidities between the ages of 28 and 55 years with an average age of 41.7

years and an average body mass index of 24.4 as described previously (Supporting Information Table 1) [31]. Informed consent was obtained before the liposuction procedure and local institutional review board approval preceded all human investigation. Mouse DM cells were harvested from skulls of 3-day-old and 60-day-old mice (n = 10 mice) as described previously [33]. Passage 2–6 cells from DM were used for all experiments.

hASC Labeling

For select in vivo experiments to verify viability, hASCs were stably transduced with the lentivirus carrying triple fusion reporter genes, including firefly luciferase (*Fluc*), green fluorescent protein (*GFP*), and herpes simplex virus truncated thymidine kinase (*HSV-ttk*) genes. Cells were purified by Fluorescence-activated cell sorting based on GFP expression.

In Vitro Culture Assays

For osteogenic differentiation, juvenile and adult mouse DM and hASCs were seeded either in coculture or in CM experiments. Coculture assays were performed as described previously [34]. On attachment, transwell inserts were combined and medium was replenished with either standard growth medium (SGM) or osteogenic differentiation medium (ODM) [35]. All assays were performed in triplicate. CM was obtained from DM, mouse osteoblasts (mOBs), or hASCs as described previously [36]. Briefly, cells were seeded at a density of 800,000 cells in a 10-cm plate. Approximately 24 hours was allowed for attachment, and subsequently, serum free Dulbecco's modified Eagle's medium (DMEM) was placed on the cells for a period of 24 hours. After this period, the media was collected and the cells were counted. Media was normalized to cell number and then concentrated 100 ×. For our enzyme-linked immunosorbent assay (ELISA), this was used directly, and for CM treatment, this CM was brought back to 1 × volume with ODM.

After attachment, cells were treated with ODM. Cells were maintained for 7 days in ODM with the media changed every other day. To assess early osteogenesis, alkaline phosphatase (ALP) and Alizarin Red staining and quantification were performed at 3 and 7 days, respectively, as described previously [37]. Vehicle control for rhBMP-2 or anti-BMP-2/4 treated cells was 0.01% bovine serum albumin. Proliferation of hASCs with and without DM CM was assessed by cell counting and bromodeoxyuridine (BrdU) incorporation as described previously [35].

Preparation of Scaffolds

Apatite-coated poly(lactic-co-glycolic acid) (PLGA) scaffolds were fabricated from 85/15 PLGA by solvent casting and a particulate leaching process as described previously [38, 39]. For BMP-2 loaded scaffolds, rhBMP-2 (Medtronic, Minneapolis, MN, www.medtronic.com) was adsorbed onto fabricated scaffolds by dropping protein solution onto the scaffolds for 20 minutes and further lyophilized on a freeze drier (Lab-conco, Kansas City, MO) overnight. BMP-2 (1.25 μ*g*) was applied to our scaffold, which had a volume of 6.28 μl giving a final concentration of 200 μg/ml. For antiBMP-2/4 scaffolds, 126 ng of human BMP-2/BMP-4 antibody (MAB3552, R&D, Minneapolis, MN) was adsorbed (final concentration of 20 μg/ml) onto fabricated scaffolds by dropping protein solution onto the scaffold for 20 minutes and further lyophilized on a freeze drier.

Creation of Calvarial Defects

After anesthesia, an incision was made just off the sagittal midline, and the periosteum was completely removed from the right parietal bone of adult (60-day-old) male Crl:NU-Foxn1^{nu} CD-1 nude mice [31]. A unilateral 4 mm full-thickness defect was created in the nonsuture associated right parietal bone. The underling DM was either meticulously preserved or a 4-mm round injury in the DM was created (Supporting Information Fig. 1A).

In preparation for cell engraftment, scaffolds were seeded with hASCs 24 hours before implantation [31]. Animals were divided equally into 10 treatment groups (n = 5 mice per group): (a) empty defects, (b) scaffold alone, in which a scaffold without cells was placed in the defect site, (c) hASCs on a scaffold, in which hASCs were impregnated in a scaffold which was then placed in the defect site with intact DM, (d) hASCs on a scaffold, in which hASCs were impregnated in a scaffold which was then placed in the defect site with DM carefully dissected off of the entire 4 mm defect site, (e) hASCs on a BMP-2 loaded scaffold (200 μg rhBMP-2), placed in the defect site with DM carefully dissected off of the entire 4 mm defect site, (f) hASCs on a BMP-2 loaded scaffold, with intact DM (g) hASCs on a PLGA scaffold with a nonpermeable 6 mm diameter, 0.01 inch thick, silicone membrane (Siltex, Pillar Surgical, LA Jolla, CA) placed below the calvarial defect overlying the DM, thus separating the scaffold from the underlying DM, (h) scaffold without hASCs placed on a nonpermeable silicone membrane, (i) a nonpermable silicone membrane placed with no overlying scaffold or hASCs, and (j) hASCs on a scaffold placed on a semipermeable membrane (6 mm diameter, pore size 0.4 μM) (Corning Incorporated, NY). In additional experiments, the following groups were added: (a) hASCs on an antiBMP-2/4 loaded scaffold with DM intact and (b) anti-BMP-2/4 loaded scaffold without cells with DM intact. Finally, the skin was sutured and animal monitored per established postoperative protocols.

In Vivo Imaging

Micro–X-ray computed tomography (micro-CT) was performed on live animals in a serial manner postoperatively (through 8 weeks healing), using a high-resolution MicroCAT II (ImTek Inc., Knoxville, TN, www.imtek.com) small animal imaging system as described previously [31]. For In Vivo Imaging System (IVIS), mice were anesthetized and luciferin (150 mg/kg in 200 μl) injected into the peritoneal cavity. After 10 minutes, animals were then placed in the IVIS 200B imaging system and imaged for 3 minutes as described previously [40].

Histologic Analyses

Animals were sacrificed for histology and prepared as described previously [31]. Histomorphometry of each aniline blue section was performed as described previously [41]. Next, select slides were stained with Pentachrome, in which mature bone appears bright yellow. ALP staining was performed on select slides [41, 42]. In situ hybridization (ISH) was performed on select slides for *Bmp-2*, *Runx-2*, osteocalcin (*Ocn*) [41]. Nonspecific binding was minimized by high stringency hybridization conditions, for all assays sense probes were used side-by-side with minimal background.

Cellular proliferation was assessed by BrdU immunohistochemical staining (Zymed, South San Francisco, CA, www.invitrogen.com). BrdU labeling was quantified by taking five representative images of the region of the defect at 10 × (spanning the entire defect). 3,3′-Diaminobenzidine (DAB) positive bone per × 10 field was quantified, (n = 5 slides per group), three animals per group using Adobe Photoshop. Data was normalized to the DM removed group.

IHC of SMAD Pathway and OCN

Immunohistochemistry (IHC) was performed on selected slides that were deparaffinized and rehydrated. Endogenous peroxidase activity was quenched with 3% hydrogen peroxide in methanol; slides were blocked with 10% goat serum in phosphate-buffered saline. Antibodies used included rabbit major histocompatibility complex 1, polyclonal anti-SMAD-1, (1:80 in dilution, Santa Cruz Laboratories, Santa Cruz, CA), rabbit polyclonal anti-pSMAD-1 (1:80 in dilution, Santa Cruz Laboratories), or rabbit polyclonal anti-Ocn 1:80 in dilution (Santa Cruz Laboratories) and were suspended in 1% rabbit serum. Appropriate biotinylated secondary antibodies were used in 1:1,000 dilution (Vector Laboratories, Burlingame, CA, www.vectorlabs.com). The Vectastain ABC system (Vector Laboratories) was used according to the manufacturer's instructions. Visualization was with diaminobenzidine solution (Zymed Laboratories, South San Francisco, CA). Slides without primary antibody were used as a negative control.

Immunofluoresence for Colocalization of Human Nuclear Antigen, OCN, and Wnt1A

Sections were incubated in human nuclear antigen (Thermo Scientific Pierce Antibodies, www.thermo.com; #MA1–83365), *Ocn* (AbCam, www.abcam.com; ab14173), or human specific *OCN* (hOCN) was used (US Biological, Swampscott, MA; 0860) and Wnt1 (AbCam-ab15251) primary antibodies at 4°C overnight, followed by incubation with Alexa Fluor 594 goat anti-rabbit secondary antibody (Invitrogen, 1:400) and Alexa Fluor 488 anti-mouse for 1 hour. Cover slips were applied with Vectashield Mounting media (Vectorlabs) and analyzed with fluorescence (Axioplan, Zeiss); slides without primary antibody along with slides with nonspecific monoclonal antibodies were used as a negative control. No less than five slides were stained for each antibody per time point and imaged with a confocal fluorescence microscope (Leica DM IRE2).

Immunofluoresence of GFP

Sections were incubated in GFP primary antibody at 4°C overnight, followed by incubation with Alexa Fluor 594 goat anti-rat secondary antibody (Invitrogen, 1:400) for 1 hour. Cover slips were applied with Vectashield Mounting media (Vectorlabs) and analyzed with fluorescence (Axioplan, Zeiss); slides without primary antibody were used as a negative control. No less than five slides were stained for each antibody per time point and imaged with a confocal fluorescence microscope (Leica DM IRE2).

Quantification of BMP-2 Protein in DM Cells and CM

To quantify the BMP-2 present in DM cells and their cell CM, a double sandwich ELISA was used, purchased from R&D Systems (Minneapolis, MN).

Western Blot Analysis of BMP Signaling Pathway

Subconfluent hASCs were treated with SGM, ODM, ODM with DM CM, or ODM with DM CM and a BMP-2/4 inhibitory antibody (BMPi) for 3, 6, and 12 hours. Concurrently, hASCs were treated with or without overlying DM cells for 3, 6, and 12 hours. Then the hASCs were washed and lysed with cold lysis buffer containing 1 mmol/l of sodium orthovanadate and Protease Inhibitor Cocktail (Sigma-Aldrich, St. Louis, MO, www.sigmaaldrich.com). Cell lysates were assayed for protein concentration by BCA assay. Aliquots (50–100 μ*g*) of cell lysate were electrophoresed on 12% Tris-HCl SDS-sodium dodecyl sulfate polyacrylamide gel electrophoresis gels (Precast Nupage gels, Invitrogen, Life technologies) and transferred onto Immobilon-P membrane (Millipore Corporation, Bedford, MA, www.millipore.com). Antibodies against the specific phosphorylated and nonphosphorylated proteins were chosen as follows: anti-pSMAD 1/5 and SMAD-5 (Cell Signaling, www.cellsignal.com, 9516 and 9517). For our analysis of the adult and juvenile DM, cells were plated at a density of 800,000 cells per 10 cm plate and allowed 24 hours for attachment. Subsequently, cells were treated with ODM for 0, 3, 6, and 12 hours, harvested and analyzed for BMP-2 (AbCam-ab14933). A horseradish peroxidase-conjugated anti-rabbit antibody 1:8,000 was used as secondary antibody. Immunoblotted products were visualized by enhanced chemiluminescence substrate (Amersham Biosciences, UK, www.gelifesciences.com). All bands of the phosphorylated or nonphosphorylated proteins in the immunoblots were normalized with the loading controls (α-tubulin) and quantified by densitometry.

Polymerase Chain Reaction

Total RNA was isolated from cells and tissue as described previously [35, 41]. Quantitative real-time polymerase chain reaction (qRT-PCR) was carried out using the Applied Biosystems Prism 7900HT Sequence Detection System and Sybr Green PCR Master Mix (Applied Biosystems, www.applied-biosystems.com). Specific primers for the genes examined were based on their PrimerBank sequence and are listed in Supporting Information Table 2. The levels of gene expression were determined by normalizing to values of mouse or human glyceraldehyde 3-phosphate dehydrogenase (*GAPDH*) and performed in triplicate.

Statistical Analysis

Means and SDs were calculated from numerical data, as presented in the text, figures, and figure legends. In figures, bar graphs represent means, whereas error bars represent one SD. Statistical analysis was performed using an appropriate analysis of variance when more than two groups were compared, followed by a post hoc Student's *t* test (with a Bonferroni correction) to directly compare two groups. The exact statistical analysis for each dataset is described in the figure legends. Inequality of SDs was excluded by using the Levene's test. *p* values are included in the figure legends.

Results

hASCs Require Interaction with DM for Calvarial Healing

First, we confirmed that hASCs were capable of healing a critical sized calvarial defect with the DM intact, as observed previously (Fig. 1) [43]. As early as 2 weeks postoperative, hASC-engrafted defects exhibited islands of bony regenerate (Fig. 1A, third row). By 4 weeks, the majority of the hASC-engrafted defects with an intact DM showed robust healing (Fig. 1A, third row, 1B). These findings were in comparison with control groups either left empty (Fig. 1A, first row) or “scaffold alone” without hASCs (Fig. 1A, second row). The control of scaffold alone is of specific importance because DM cells are also known to be able to undergo osteogenic differentiation [44]. However, clearly, in this adult mouse model, the DM cells without overlying hASCs are insufficient to allow for greater than 15% healing of the defect at 8 weeks (Fig. 1B).

To interfere with the DM-hASC interaction, two methods were used. First, we performed a careful removal of all DM in the defect site by meticulous microdissection before placement of the hASC-engrafted scaffold (Supporting Information Fig. 1). Approximately 8-week histology demonstrated that the DM was indeed missing along the length of the defect and had not regenerated in its original position (Supporting Information Fig. 1C, bottom left vs. bottom right). As a second, nontraumatic methodology, an impermeable silicone membrane was placed between the hASC-engrafted scaffold and intact underlying DM. Either method to disrupt the DM-hASC interface significantly reduced bony healing (Fig. 1A, fourth and fifth rows, 1B). Neither DM excluded group demonstrated more than 25% healing and both groups exhibited significantly less healing than those defects treated with an hASC seeded scaffold at both early (2 weeks postoperative) and late time points (4 and 8 weeks postoperative). Further controls included implantation of the impermeable silicone membrane alone, as well as the impermeable silicone membrane with a scaffold and no cells, which as expected showed minimal healing (Supporting Information Fig. 2A). Interestingly, mice with the silicone barrier failed to show significant healing regardless of whether an osteoconductive scaffold alone or an osteoconductive scaffold with hASCs was placed over the top of the barrier (Fig. 1A, fifth row, 1B, and Supporting Information Fig. 2). If the primary pro-osteogenic effect of DM cells on hASCs is via the delivery of soluble paracrine factors, then the introduction of a semipermeable rather than an impermeable membrane should not interfere to the same extent with calvarial healing. Indeed, we found this to be the case: although not as robust of healing as with intact DM without insertion of a membrane, bony islands were observed within hASC-engrafted defects after semipermeable membrane insertion (Fig. 1A, sixth row). Results from micro-CT were quantified and presented as average fraction healing of the original defect size, showing clearly that the unperturbed DM-hASC interface was necessary for normal hASC mediated healing (Fig. 1B, gray bar vs. purple bar). Furthermore, quantification of calvarial healing demonstrates significantly more healing in those defects where a semipermeable membrane was placed under the hASC scaffold than when the DM-hASC interface was completely disrupted (Fig. 1B, green vs. blue).

Histological analysis was performed at 8 weeks postoperatively to confirm micro-CT findings. Consistent with radio-graphic analysis, hASC-engrafted defects with intact DM showed significant bony regenerate as shown by aniline blue and pentachrome staining (Fig. 2C, third row). The bone formed was noticed to be thick osteoid that spans the entire scaffold and is not just along the interface between the DM and scaffold. In contrast, when DM was surgically removed before hASC-engrafted scaffold placement, little ossification was observed 8 weeks postoperatively (Fig. 2D). Similarly, a complete lack of bone is noted if a nonpermeable membrane is placed between the underlying DM and the hASC seeded scaffold (Fig. 2E). Between these two extremes, the defect with a semipermeable membrane between the DM and overlying scaffold with hASCs allowed for some osteoid formation both above and below the membrane, although not as much as those defects without any membrane (Fig. 2F). When we measured the amount of osteoid formed, by quantifying the amount of aniline blue pixels by histomorphometric analysis of serial sections rather than the percent of the defect healed (as done with the micro-CT scans), we also noted large differences in our treatment groups with the ASC seeded scaffold over an intact DM having significantly more bone than those defects with a disrupted DM/hASC interface. The semipermeable membrane group formed bone at levels between these groups (Fig. 2G). Finally, ALP activity was assessed in vivo, as indicated by purple staining. Consistent with our other findings, ALP stain was seen in those defects with an intact DM and not in those with the DM/scaffold interface disrupted (Fig. 2C, 2D, fourth column).

hASCs and Underlying DM Cells Participate in the Osseous Regeneration

To demonstrate that the implanted Luc^{+}/GFP^{+} hASCs persisted at 2 weeks (a time point with a robust increase in bone formation), we performed luciferase imaging, immunofluoresence for GFP demonstrating presence of the human donor cells in the defect (Supporting Information Fig. 3A, 3B). Once persistence was confirmed, we next set out to explore participation of hASCs and DM cells in the osseous regeneration. The proto-oncogene Wnt1 has been shown to encode for a short range signal that is only expressed during the development of the central nervous system [45–47]. Furthermore, a transgenic Wnt1-lacZ transgenic mouse has been used to follow the migration and differentiation of neural crest cells [20, 48]. Thus, we set out to assess Wnt1 expression as a marker for DM cells which are neural crest derived. Using Wnt1/Cre transgenic mouse, our laboratory has demonstrated previously that in an untreated calvarial defect, cells from the DM migrate into the region of the defect [49]. Our current study uses human cells preventing us from using this immunocompetent mouse strain, and thus, we set up a series of experiments in our nude mouse model to demonstrate both human and mouse contribution to the bony regeneration. First, we performed immunofluoresence for mouse Wnt-1 protein which is known to be found in neural crest cells (present in the DM) and demonstrate that these cells localize to osteoid in the defect and colocalize with OCN using confocal microscopy (Supporting Information Fig. 3C). Next, to verify human participation in the same region of new bone formation, we performed immunofluorescent staining for a human specific nuclear antibody as well as hOCN. Using confocal microscopy, we demonstrate that indeed there is colocalization of the human nuclear antigen and hOCN in the region of new osteoid (Supporting Information Fig. 3D). Next, designed mouse and human specific ISH probes for Ocn. Interestingly, we found that the mOcn probe had a high signal along the DM interface,

whereas the hOCN had a higher signal near the superior part (away from the DM) of the scaffold (Supporting Information Fig. 3E). Thus, it appears that mouse host cells contribute, especially along the base of the scaffold. To further explore the contribution of the DM, we designed a mouse specific Wnt1 probe and compared expression in those defects with the DM intact compared to those defects with the DM removed both with overlying scaffold with ASCs. We demonstrate significant signal in those defects with the DM intact and minimal signal in the defect with the DM removed (Supporting Information Fig. 3F). Finally, we assessed for bone formation under both nonpermeable (prevents cell and protein migration) and semipermeable membrane (allowed proteins migration, prevents cell migration). We demonstrate thick osteoid under the semipermeable membrane, which most likely originated from the DM because the hASCs could not migrate through the membrane (Supporting Information Fig. 3G). Interestingly, this bone under the membrane is only seen in the semipermeable-permeable membrane group and not the nonpermeable membrane group (Supporting Information Fig. 3G second vs. third row) indicating that the DM likely requires a paracrine interaction from hASCs to undergo osteo-genic differentiation. Thus, we demonstrate using several methodologies that the de novo bone formed in the calvarial defect has contributions from both the underlying DM cells and the implanted hASCs and are likely dependent on paracrine interactions with each other.

DM Cells Induce Proliferation of hASCs

After demonstrating both persistence of hASCs and improved healing of defects treated with hASCs, we hypothesized a paracrine effect that mediated the DM-hASC interaction—we next turned to in vitro studies to more thoroughly define this relationship.

DM is a known source of mitogenic growth factors [33]. Previous studies have demonstrated that the DM stimulates osteoblast proliferation [33]. Therefore, we first hypothesized that DM cells stimulate hASC proliferation via a paracrine interaction. CM obtained from DMs was observed to significantly increase hASC proliferation in vitro, as assessed by cell counting assays (Fig. 3A) and BrdU incorporation assays (Fig. 3B). We also found that DM created a mitogenic niche in vivo as well. *Pcna expression* within calvarial defect site was significantly reduced when the DM was removed (Fig. 3C). Similarly, BrdU immunostaining and quantification of labeled specimens either with DM intact or DM removed demonstrated a higher BrdU incorporation in those defects with an intact DM (Fig. 3D, 3E). Thus, a calvarial defect with intact DM provides a mitogenic environment for transplanted cells in their proximity.

DM Cells Induce Osteogenic Differentiation of hASCs

Along with providing a source of mitogenic factors, DM is also a known source of pro-osteogenic cytokines [50]. We have demonstrated previously that significantly more healing occurs when a semipermeable membrane rather than a non-permeable membrane is placed between the underlying DM and the overlying hASCs (Fig. 1). This difference in healing suggests that the DM has a paracrine effect on the engrafted hASCs. We next hypothesized that DMs will enhance hASC osteogenic differentiation in vitro (Fig. 4). This was tested using both a noncontact coculture and CM assays. Briefly, co-culture of hASCs with DMs significantly enhanced hASC osteogenesis. First, we assessed the effect of culturing DM

cells in a transwell with a semipermeable membrane (0.4 μM) above hASCs, allowing only the movement of secreted proteins with no cells. To assess early osteogenesis, we performed an ALP stain and quantification after 3 days of treatment with or without coculture conditions, demonstrating significantly higher ALP levels in those ASCs cultured with DM cells (Fig. 4A, 4B). To assess late osteogenic effects and bone nodule formation, we performed an Alizarin Red stain and quantification after 7 days with or without coculture conditions. Again, hASCs demonstrated significantly more calcium deposition when cocultured with DM cells (Fig. 4C, 4D). To correlate our ALP stain with gene expression at 3 days, we performed qRT-PCR for *ALP*, *RUNX-2*, and *OCN*. hASCs had significant upregulation of *ALP*, *RUNX-2*, and *OCN* when cultured with DM cells (Fig. 4E).

Next, we set out to examine if the DM cells secreted proteins that, when applied to hASCs, increased their osteogenic capacity. Similar to our coculture results, application of DM CM significantly increased early ALP stain and quantification (Fig. 4F, 4G), as well as calcium deposition, as assessed by Alizarin Red stain and quantification (Fig. 4H, 4I). Gene expression was consistent with these stains as hASCs exposed to DM CM showed an upregulation of *ALP*, *RUNX-2*, and *OCN* (Fig. 4J). Thus, DM cells clearly secrete soluble proteins that stimulate the osteogenic differentiation of hASCs.

Juvenile DM Cells Induce Greater Osteogenic Differentiation in hASCs Than Adult DM Cells

Our laboratory has demonstrated previously that juvenile as compared to adult DM cells induce greater proliferation and osteogenic differentiation in osteoblasts when placed in a co-culture environment [51]. Thus, we set out to demonstrate if the difference in age of the DM had a similar effect on hASCs. We found that hASCs in coculture with juvenile DM cells demonstrated a greater amount of ALP stain and quantification after 3 days in ODM as well as increased mineralization by Alizarin Red at 7 days of differentiation (Supporting Information Fig. 4A–4C). We next assessed osteogenic gene expression and noted a similar trend with the hASCs exposed to juvenile DM cells expressing higher level of osteogenic genes including *ALP*, *RUNX-2*, *OCN*, and *BMPR1B* (Supporting Information Fig. 4D). In addition, we explored the *Bmp-2* expression of adult and juvenile DM cells independent of the hASC coculture. We noted, that the juvenile DM cells demonstrated higher expression of BMP-2 protein at baseline and after 3, 6, and 12 hours after treatment with ODM (Supporting Information Fig. 4E, 4F), which was consistent with previous studies [10]. Thus, if we are to harness, the osteogenic capability of juvenile DM in adult defects, BMP-2 should be supplemented.

hASCs Induce Osteogenic Differentiation of DM In Vitro

Having observed the paracrine effects that DM cells have on hASCs, the converse relationship was also assayed. Using the same techniques of coculture, the effects of hASCs on DM osteogenic differentiation was assessed. Alizarin Red staining at 14 days differentiation showed that hASCs cocultured with DM had a significant pro-osteogenic effect on the DM cells (Supporting Information Fig. 5A, 5B). Results were verified by qRT-PCR, showing significant increases in mouse osteogenic gene marker levels with the addition of the coculture environment (*Bmp-2*, *Bmpr1b*, *Runx-2*, and *Ocn*; *, $p < .05$)

(Supporting Information Fig. 5C). Thus, it is likely that DM cells, which are neural crest derived and osteocompetent, display a more enhanced osteogenic capability when exposed to hASCs. This was consistent with our in vivo data that DM-derived bone formed under the semipermeable membrane when overlying hASCs were placed but not when nonpermeable membrane was placed between the DM and overlying hASCs (Supporting Information Fig. 3G).

The Pro-Osteogenic Effect of DM Cells on hASCs Is Dependent on BMP-2 Signaling

As reported previously, we first confirmed [52] that rhBMP-2 significantly enhanced hASC osteogenic differentiation under standard in vitro conditions (Supporting Information Fig. 6). Next, we assessed the amount of BMP-2 secreted by DM cells using a protein ELISA and compared the amount of BMP-2 secretion by DM cells with that of mOBs and hASCS. We seeded 800,000 DM cells in a 10-cm dish and allowed 24 hours for attachment. Subsequently, 10 ml of serum free DMEM was placed on the DM cells for 24 hours and then collected and concentrated 100 ×. After the CM was collected, cell counting was performed to allow for normalization of the ELISA. CM collected from DM cells was observed to secrete significantly higher levels of BMP-2 than hASCs, reaching levels close to that of our positive control, mOBs. (Fig. 5A). To determine if this robust BMP-2 ligand production by DM cells had an effect on hASCs, we performed a western blot analysis to measure the downstream signaling effects of the BMP-2 pathway in DM-hASC coculture or CM experiments. We found increased hASC downstream BMP signaling transduction, as assessed by Western blot for pSMAD 1/5 upon coculture of hASCs with DMs after 3, 6, and 12 hours in culture (Fig. 5B). We subsequently manipulated this pathway by adding the CM to ODM (brought the 100 × to volume in ODM and normalized to cell number) or a BMP-2/4 antibody and demonstrate that while SMAD 5 protein levels remain constant, there is a significant decrease in the activated or phosphorylated form of SMAD-1/5 when the BMP-2/4 antibody was added to the CM-treated cells which was most dramatic at 3 hours (Fig. 5B–5D). To further assess downstream BMP signaling, we performed qRT-PCR for *RUNX-2* of hASCs cultured with or without DM cells after 3, 6, and 12 hours in culture, demonstrating that hASCs cultured with DM cells have significantly higher expression of *RUNX-2* likely due to downstream signaling by pSMAD-1/5 (Fig. 5E).

Next, we assayed BMP ligand and receptor expression in hASCs post-DM stimulation, by qRT-PCR. Both coculture and CM conditions increased hASC expression of *BMP-2*, and *BMPR1B*, results suggestive of DM-derived BMP induction in responding hASCs (Fig. 5F, 5G).

Having demonstrated the secretion of BMP-2 by DM cells and its osteogenic effect on hASCs, we assessed the extent to which this pro-osteogenic effect of DMs on hASCs was dependent on BMP-2 signaling. To do this, a neutralizing BMP-2/4 antibody was incubated with the DM CM and subsequently used to treat hASCs during osteogenic differentiation (Fig. 5H–5K). By all markers examined, addition of a neutralizing BMPi antagonized the pro-osteogenic effect of DM CM on hASCs. Thus, we concluded that the in vitro pro-osteogenic effect of DM on ASCs is primarily via BMP-2 signaling. Thus, we would

hypothesize that in vivo, DM cells would also create an osteogenic niche by providing factors such as BMP-2.

DM Enhances the Early Osteogenic Environment of a Calvarial Defect, Accompanied by Increased BMP-2 Signaling

Having demonstrated a likely role for BMP-2 signaling in DM stimulated hASC osteogenesis, we returned to in vivo calvarial defects to define the effect of DM removal on the early, postoperative osteogenic microenvironment. To this end, 4 mm calvarial defects were made in the parietal bone of 60-day-old nude mice. The DM was either left intact or carefully dissected off the entirety of the defect site. We were first interested in the environment created by the DM cells alone as no hASCs or scaffolds were placed in the defect. On postoperative day 5, specimens were examined, allowing for assessment of the early wound environment (Fig. 6A).

Indeed, surgical removal of DM led to a clear reduction in BMP ligand expression and BMP signaling activity. This was demonstrated by ISH for *Bmp-2* (second column) and immunohistochemical staining for pSMAD-1 (sixth column) (Fig. 6A). Similarly, there was an upregulation in osteogenic genes and proteins as demonstrated by increased stain in for *Runx-2* and *Ocn* in those defects with the DM intact (Fig. 6A, third to fifth columns).

Having demonstrated that the DM osteogenic capacity is upregulated by injury and that the presence of the DM creates an osteogenic environment, we next set out to investigate how the intact DM would affect signaling of the overlying hASCs. We found that the presence of DM led to greater osteogenic gene expression by ISH and enhanced signaling through the SMAD-1/5 pathway (Fig. 6B). IHC performed 5 days after calvarial defect creation with both an intact DM demonstrated higher immunoreactivity for pSMAD-1 as well as Ocn (Fig. 6B). To verify these analyses, a similar defect was created and the DM was either kept intact or dissected off the underlying brain. Approximately 5 days after the injury, tissue from the defect (excluding the surrounding calvaria and brain) was carefully dissected and RNA was harvested (n = 5 mice per defect). *Bmp-2*, *Bmp-4*, and *Bmpr1b* expression were all significantly upregulated in those defects with the DM intact when compared with those with the DM removed (Fig. 6C).

Next, we explored whether this osteogenic effect seen by the DM was innate or whether its osteogenic nature was elicited by calvarial injury. To do this, we assessed ISH expression of Bmp-2 in the region under the calvarial defect when compared with the uninjured contralateral parietal bone (Fig. 6D). We found that the expression of these osteogenic genes was present in both regions; however, a larger region of expression is noted under the injured parietal bone indicating that the osteogenic nature of the DM appears to be enhanced by calvarial injury.

As the surrounding osteoblasts are also a known osteogenic cell type, we also analyzed the wound edges by ISH to determine if there was also a difference in gene expression of these cells after calvarial injury. Interestingly, we found that there was no difference in gene expression of Bmp-2, Runx-2, or Ocn in the bony edges with or without a DM injury (Fig. 6E). Thus, the difference in gene expression and signaling in the calvarial defect was likely

due to differences created by the DM rather than the surrounding osteoblasts. In summary, we demonstrate that the critical size calvarial defect demonstrates enhanced osteogenic gene expression and protein production when the DM is left intact, which is maintained when a hASC seeded scaffold is placed in the defect. Furthermore, this osteogenic nature of DM does appear to be elicited by calvarial injury.

BMP-2 Inhibition Makes the Calvarial Defect "Dural-Injury-Like," Whereas BMP-2 Supplementation "Rescues" hASC-Mediated Calvarial Healing After DM Removal

Our in vivo and in vitro experiments suggest that the DM-hASC paracrine interaction result in a profitable enhancement of osteogenic differentiation via BMP signaling. Thus, if the primary pro-osteogenic, DM-derived cytokine is BMP-2, then inhibition of BMP-2 through a slow releasing antiBMP-2 scaffold should mitigate the osteogenic effect of the DM cells. To explore this idea, we constructed an anti-Bmp-2/4 scaffold (20 μg/ml), seeded with hASCs as in previous experiments and implanted this scaffold into our critical size defect model. By micro-CT scan, these scaffolds significantly inhibit osteogenic healing of the calvarial defect as there was less than 25% healing as far as 6 weeks (Supporting Information Fig. 7A, 7B). Concurrently, this inhibitory antibody caused a decrease in BMP-2 signaling as shown by pSMAD-1 expression on IHC (Supporting Information Fig. 7C). Similarly, Ocn levels were also lower in those defects with the anti BMP-2/4 scaffold implanted.

More importantly from a clinical standpoint, the addition of recombinant BMP-2 should stimulate hASC-mediated healing even in the absence of DM. To investigate this question, BMP-2 (1.25 μg or 200 μg/ml, given scaffold volume of 6.28 μl) was loaded into scaffolds before cell engraftment (Fig. 7). We demonstrate that these scaffolds allow for an initial pulse release of 30% of the BMP-2 during the first 2 weeks, followed by a period of slow release for 4 weeks in vitro (data not shown). This scaffold was again seeded with 150,000 hASCs and placed in a 4-mm calvarial defect with either intact or removed DM. Indeed, BMP-2 supplementation augmented calvarial healing in the defect site with the underlying DM intact (Fig. 7A second row vs. third row, 7B). Similarly, the BMP-2 scaffold allowed for more than 80% healing of a calvarial defect even in the absence of the underlying DM (Fig. 7A, fourth row, 7B). This is more healing than was noted in the hASC seeded non-BMP-2 scaffold, where only 20% healing was observed at 8 weeks (Fig. 1A, fourth row). Thus, the addition of rhBMP-2 could mitigate the loss of DM and lead to successful defect healing. Furthermore, the regeneration of calvarial defects with impaired healing can be augmented by recreating or supplementing the environment cues provided by the underlying DM.

Discussion

A calvarial defect is a unique niche or microenvironment for bone healing. It is composed of surrounding calvarial osteo-blasts, overlying periosteum, underlying DM, and engrafted stem cells if applicable. DM cells have long been recognized to play a significant role in calvarial healing [53–56]. For example, if DM cells are labeled in transgenic mice (using a Wnt1/cre/R26 reporter system), significant osseous repair is derived from the DM tissue

itself [49]. DM has been shown to have unique properties in the juvenile animal, including a high predilection for osteogenic differentiation [5, 7, 33, 51, 57, 58]. These studies suggest that the ability for young patients to heal large calvarial defects may arise from the intact DM beneath the skull. In numerous studies, DM retain the ability to form bone or bone nodules, either when cultured in vitro and implanted ex vivo [56]. In addition, numerous studies have examined the pivotal role that DM plays in a paracrine fashion to influence the overlying skull [59, 60]. Dura plays a role in intramembranous ossification of the skull vault, and later in development plays a role in dictating cranial suture fate (or suture fusion vs. patency) through regional specification of DM tissue [61]. For example, we have previously found through surgical manipulation that cranial suture fusion can be reversed or patency interrupted if the suture-DM interface is manipulated [59, 60, 62, 63]. These studies offered significant insight into the osteogenic role of DM cells on their surrounding tissues in several biologic scenarios (cranial bone defects and cranial suture fusion among others).

Despite their known role as an osteocompetent and osteoinductive cell type, DM cells fail to heal a calvarial defect in adults [1, 3–8, 64, 65]. Thus, this study sought to address whether DM tissue had an influence on hASCs when engrafted into a calvarial defect. Thus, numerous studies have examined the difference between the osteogenic and mitogenic capacity of adult versus juvenile DM. In both a static noninjured calvarium and in a defect model, juvenile DM has been shown to express greater levels of BMP-2 [7, 10]. Furthermore, transplantation of juvenile DM to an adult defect has been shown to stimulate osseous healing in an otherwise nonhealing defect [5]. Our findings corroborate these previous studies and demonstrate that the juvenile DM has a more osteogenic effect on hASCs in vitro as well. However, for human adult patients with nonhealing calvarial defects, DM cells are not an available or a realistic cell type for tissue engineering. Thus, we set out to make our adult mouse calvarial defect more “juvenile-like” by engrafting hASCs, which are known to respond to BMP-2, and have been shown to be osteogenic in vivo [31, 52]. To further enhance the osteogenic niche of the calvarial defect, we also provided BMP-2 protein through a slow releasing scaffold.

In our study, we identified that BMP-2 augmented calvarial healing if the DM mater was disrupted and further demonstrated the role of BMP signaling in this DM-hASC paracrine interaction. BMP signaling, first recognized to stimulate ectopic bone formation, has since been shown to be important in osteogenic differentiation of ASCs [29, 66–69]. In fact, BMP signaling via the receptor Bmpr1b has been shown to be necessary for mASC osteogenic differentiation, as siRNA-mediated knockdown inhibited their ability to undergo osteo-genic differentiation [67]. Specifically, while BMP signaling was the focus of this current study, there is no doubt that other DM-derived signaling cascades likely work in concert with the BMP pathway to promote calvarial healing. These other factors such as FGF-2, insulin-like growth factor, TGF-β, Hedgehog, or Wnt signals, to name a few, may be the focus of future investigation [10, 57, 65, 70–75].

Our study focused on the manner in which host mouse DM may both participate and stimulate donor hASC reossification of the calvarium in a nude mouse. There is no doubt that our nude mouse model might have different healing capabilities than immunocompetent mice. Bone repair occurs as a result of participation by the immune and hematopoetic niche

of immune marrow cells and osteogenic precursors from surrounding tissues [34, 76, 77]. Nude or athymic animals may demonstrate a blunted inflammatory response; however, they only lack a T-cell response and can still mount an inflammatory response with regards to B-cells and NK-cells and still possess the surrounding osteogenic precursor cells from the DM. We chose to use our nude mouse model rather than immunocompetent strain as we were using human cells and because we have established and verified this model in previous studies thus offering the most controlled design [31, 36, 78].

There are other intriguing cell-cell paracrine interactions that may be explored. In our previous study, we examined the mOB-hASC interaction in the same calvarial defect model [34]. Other studies have also analyzed the contribution of the periosteum versus the DM in calvarial ossification and have demonstrated the relative importance of DM over periosteum [5, 56].

Conclusion

In conclusion, hASCs heal critical-sized calvarial defects only when the underlying DM is left intact. Our studies suggest that DM-derived BMP signaling is at least in part necessary for hASC-mediated calvarial healing. Moreover, in future clinical scenarios with DM disruption, pro-osteogenic cytokines such as BMP-2 should be used along with ASC-mediated bony repair.

Supplementary Material

Refer to Web version on PubMed Central for supplementary material.

Acknowledgments

We thank the Stanford University Plastic Surgery Center staff, Drs. Timothy Doyle, and Victor Wong. This study was supported by National Institute of Dental and Craniofacial Research, NIH, Grants 1R21-DE019274-01 and RC2-DE020771-01 and the Oak Foundation and Hagey Laboratory for Pediatric Regenerative Medicine (to M.T.L.). B.L. was supported by the National Institute of Arthritis and Musculoskeletal and Skin Diseases, NIH, Grant 1F32AR057302 and National Endowment for Plastic Surgery.

References

1. Mabbutt LW, Kokich VG, Moffett BC, et al. Subtotal neonata calvariectomy A radiographic and histological evaluation of calvarial and sutural redevelopment in rabbits. J Neurosurg. 1979; 51:691–696. [PubMed: 501409]
2. Hanson JW, Sayers MP, Knopp LM, et al. Subtotal neonatal calvariectomy for severe craniosynostosis. J Pediatr. 1977; 91:257–260. [PubMed: 889596]
3. Mossaz CF, Kokich VG. Redevelopment of the calvaria after partial craniectomy in growing rabbits: The effect of altering dural continuity. Acta Anat (Basel). 1981; 109:321–331. [PubMed: 7293718]
4. Reid CA, McCarthy JG, Kolber AB. A study of regeneration in parietal bone defects in rabbits. Plast Reconstr Surg. 1981; 67:591–596. [PubMed: 7232579]
5. Hobar PC, Schreiber JS, McCarthy JG, et al. The role of the dura in cranial bone regeneration in the immature animal. Plast Reconstr Surg. 1993; 92:405–410. [PubMed: 8341738]
6. Mabbutt LW, Kokich VG. Calvarial and sutural re-development following craniectomy in the neonatal rabbit. J Anat. 1979; 129:413–422. [PubMed: 500496]

7. Greenwald JA, Mehrara BJ, Spector JA, et al. Immature versus mature dura mater: II. Differential expression of genes important to calvarial reossification. Plast Reconstr Surg. 2000; 106:630–638. discussion 639. [PubMed: 10987470]
8. Greenwald JA, Mehrara BJ, Spector JA, et al. Biomolecular mechanisms of calvarial bone induction: Immature versus mature dura mater. Plast Reconstr Surg. 2000; 105:1382–1392. [PubMed: 10744229]
9. Guzel MZ, Yildirim AM, Yucel A, et al. Osteogenic potential of infant dural grafts in different recipient beds. J Craniofac Surg. 1995; 6:489–493. [PubMed: 9020740]
10. Wan DC, Kwan MD, Gupta DM, et al. Global age-dependent differences in gene expression in response to calvarial injury. J Craniofac Surg. 2008; 19:1292–1301. [PubMed: 18812854]
11. Halvorsen YC, Wilkison WO, Gimble JM. Adipose-derived stromal cells–their utility and potential in bone formation. Int J Obes Relat Metab Disord. 2000; 24(suppl 4):S41–S44. [PubMed: 11126240]
12. Lendeckel S, Jodicke A, Christophis P, et al. Autologous stem cells (adipose) and fibrin glue used to treat widespread traumatic calvarial defects: Case report. J Craniomaxillofac Surg. 2004; 32:370–373. [PubMed: 15555520]
13. Mesimaki K, Lindroos B, Tornwall J, et al. Novel maxillary reconstruction with ectopic bone formation by GMP adipose stem cells. Int J Oral Maxillofac Surg. 2009; 38:201–209. [PubMed: 19168327]
14. Kulakov AA, Goldshtein DV, Grigoryan AS, et al. Clinical study of the efficiency of combined cell transplant on the basis of multipotent mesenchymal stromal adipose tissue cells in patients with pronounced deficit of the maxillary and mandibulary bone tissue. Bull Exp Biol Med. 2008; 146:522–525. [PubMed: 19489333]
15. Mao JJ, Giannobile WV, Helms JA, et al. Craniofacial tissue engineering by stem cells. J Dent Res. 2006; 85:966–979. [PubMed: 17062735]
16. Kroeze RJ, Knippenberg M, Helder MN. Osteogenic differentiation strategies for adipose-derived mesenchymal stem cells. Methods Mol Biol. 702:233–248. [PubMed: 21082406]
17. Zou J, Wang G, Geng D, et al. A novel cell-based therapy in segmental bone defect: Using adipose derived stromal cells. J Surg Res. 2011; 168:76–81. [PubMed: 20070984]
18. Bradley JP, Levine JP, McCarthy JG, et al. Studies in cranial suture biology: Regional dura mater determines in vitro cranial suture fusion. Plast Reconstr Surg. 1997; 100:1091–1099. discussion 1100–1092. [PubMed: 9326769]
19. Levine JP, Bradley JP, Roth DA, et al. Studies in cranial suture biology: Regional dura mater determines overlying suture biology. Plast Reconstr Surg. 1998; 101:1441–1447. [PubMed: 9583471]
20. Jiang X, Iseki S, Maxson RE, et al. Tissue origins and interactions in the mammalian skull vault. Dev Biol. 2002; 241:106–116. [PubMed: 11784098]
21. Gagan JR, Tholpady SS, Ogle RC. Cellular dynamics and tissue interactions of the dura mater during head development. Birth Defects Res C Embryo Today. 2007; 81:297–304. [PubMed: 18228258]
22. Quarto N, Wan DC, Longaker MT. Molecular mechanisms of FGF-2 inhibitory activity in the osteogenic context of mouse adipose-derived stem cells (mASCs). Bone. 2008; 42:1040–1052. [PubMed: 18420480]
23. Heldin CH, Miyazono K, ten Dijke P. TGF-beta signalling from cell membrane to nucleus through SMAD proteins. Nature. 1997; 390:465–471. [PubMed: 9393997]
24. Lee MH, Kim YJ, Kim HJ, et al. BMP-2-induced Runx2 expression is mediated by Dlx5, and TGF-beta 1 opposes the BMP-2-induced osteo-blast differentiation by suppression of Dlx5 expression. J Biol Chem. 2003; 278:34387–34394. [PubMed: 12815054]
25. Lee MH, Javed A, Kim HJ, et al. Transient upregulation of CBFA1 in response to bone morphogenetic protein-2 and transforming growth factor beta1 in C2C12 myogenic cells coincides with suppression of the myogenic phenotype but is not sufficient for osteoblast differentiation. J Cell Biochem. 1999; 73:114–125. [PubMed: 10088730]
26. Lee KS, Kim HJ, Li QL, et al. Runx2 is a common target of transforming growth factor beta1 and bone morphogenetic protein 2, and cooperation between Runx2 and Smad5 induces osteoblast-

specific gene expression in the pluripotent mesenchymal precursor cell line C2C12. Mol Cell Biol. 2000; 20:8783–8792. [PubMed: 11073979]

27. Peng Y, Kang Q, Luo Q, et al. Inhibitor of DNA binding/differentiation helix-loop-helix proteins mediate bone morphogenetic protein-induced osteoblast differentiation of mesenchymal stem cells. J Biol Chem. 2004; 279:32941–32949. [PubMed: 15161906]
28. Dragoo JL, Choi JY, Lieberman JR, et al. Bone induction by BMP-2 transduced stem cells derived from human fat. J Orthop Res. 2003; 21:622–629. [PubMed: 12798061]
29. Dragoo JL, Lieberman JR, Lee RS, et al. Tissue-engineered bone from BMP-2-transduced stem cells derived from human fat. Plast Reconstr Surg. 2005; 115:1665–1673. [PubMed: 15861072]
30. Peterson B, Zhang J, Iglesias R, et al. Healing of critically sized femoral defects, using genetically modified mesenchymal stem cells from human adipose tissue. Tissue Eng. 2005; 11:120–129. [PubMed: 15738667]
31. Levi B, James AW, Nelson ER, et al. Human adipose derived stromal cells heal critical size mouse calvarial defects. PLoS One. 2010; 5:e11177. [PubMed: 20567510]
32. White AP, Vaccaro AR, Hall JA, et al. Clinical applications of BMP-7/OP-1 in fractures, nonunions and spinal fusion. Int Orthop. 2007; 31:735–741. [PubMed: 17962946]
33. Li S, Quarto N, Longaker MT. Dura mater-derived FGF-2 mediates mitogenic signaling in calvarial osteoblasts. Am J Physiol Cell Physiol. 2007; 293:C1834–C1842. [PubMed: 17913846]
34. Levi B, James AW, Nelson ER, et al. Human adipose-derived stromal cells stimulate autogenous skeletal repair via paracrine hedgehog signaling with calvarial osteoblasts. Stem Cells Dev. 2011; 20:243–257. [PubMed: 20698749]
35. James AW, Xu Y, Wang R, et al. Proliferation, osteogenic differentiation, and fgf-2 modulation of posterofrontal/sagittal suture-derived mesenchymal cells in vitro. Plast Reconstr Surg. 2008; 122:53–63. [PubMed: 18594386]
36. Levi B, James AW, Nelson ER, et al. Human adipose-derived stromal cells stimulate autogenous skeletal repair via paracrine hedgehog signaling with calvarial osteoblasts. Stem Cells Dev. 2010; 20:243–257. [PubMed: 20698749]
37. James AW, Levi B, Commons GW, et al. Paracrine interaction between adipose-derived stromal cells and cranial suture-derived mesenchymal cells. Plast Reconstr Surg. 2010; 126:806–821. [PubMed: 20811214]
38. Chou YF, Huang W, Dunn JC, et al. The effect of biomimetic apatite structure on osteoblast viability, proliferation, and gene expression. Biomaterials. 2005; 26:285–295. [PubMed: 15262470]
39. Chou YF, Chiou WA, Xu Y, et al. The effect of pH on the structural evolution of accelerated biomimetic apatite. Biomaterials. 2004; 25:5323–5331. [PubMed: 15110483]
40. Levi B, James AW, Nelson ER, et al. Studies in adipose-derived stromal cells: Migration and participation in repair of cranial injury after systemic injection. Plast Reconstr Surg. 2011; 127:1130–1140. [PubMed: 21364416]
41. James AW, Theologis AA, Brugmann SA, et al. Estrogen/estrogen receptor alpha signaling in mouse posterofrontal cranial suture fusion. PLoS One. 2009; 4:e7120. [PubMed: 19771170]
42. Xu Y, Hammerick KE, James AW, et al. Inhibition of histone deacetylase activity in reduced oxygen environment enhances the osteogenesis of mouse adipose-derived stromal cells. Tissue Eng Part A. 2009; 15:3697–3707. [PubMed: 19505250]
43. Levi B, James AW, Nelson ER, et al. Human adipose derived stromal cells heal critical size mouse calvarial defects. PLoS One. 2010; 5:e11177. [PubMed: 20567510]
44. Petrie Aronin CE, Sadik KW, Lay AL, et al. Comparative effects of scaffold pore size, pore volume, and total void volume on cranial bone healing patterns using microsphere-based scaffolds. J Biomed Mater Res A. 2009; 89:632–641. [PubMed: 18442122]
45. McMahon AP, Bradley A. The Wnt-1 (int-1) proto-oncogene is required for development of a large region of the mouse brain. Cell. 1990; 62:1073–1085. [PubMed: 2205396]
46. Thomas KR, Capecchi MR. Targeted disruption of the murine int-1 protooncogene resulting in severe abnormalities in midbrain and cerebellar development. Nature. 1990; 346:847–850. [PubMed: 2202907]

47. Wilkinson DG, Bailes JA, McMahon AP. Expression of the proto-oncogene int-1 is restricted to specific neural cells in the developing mouse embryo. Cell. 1987; 50:79–88. [PubMed: 3594565]
48. Chai Y, Jiang X, Ito Y, et al. Fate of the mammalian cranial neural crest during tooth and mandibular morphogenesis. Development. 2000; 127:1671–1679. [PubMed: 10725243]
49. Behr B, Panetta NJ, Longaker MT, et al. Different endogenous threshold levels of fibroblast growth factor-ligands determine the healing potential of frontal and parietal bones. Bone. 2010; 47:281–294. [PubMed: 20472108]
50. Warren SM, Greenwald JA, Nacamuli RP, et al. Regional dura mater differentially regulates osteoblast gene expression. J Craniofac Surg. 2003; 14:363–370. [PubMed: 12826808]
51. Spector JA, Greenwald JA, Warren SM, et al. Co-culture of osteoblasts with immature dural cells causes an increased rate and degree of osteoblast differentiation. Plast Reconstr Surg. 2002; 109:631–642. discussion 643–634. [PubMed: 11818846]
52. Panetta NJ, Gupta DM, Lee JK, et al. Human adipose-derived stromal cells respond to and elaborate bone morphogenetic protein-2 during in vitro osteogenic differentiation. Plast Reconstr Surg. 2010; 125:483–493. [PubMed: 20124834]
53. Hopper RA, Zhang JR, Fourasier VL, et al. Effect of isolation of periosteum and dura on the healing of rabbit calvarial inlay bone grafts. Plast Reconstr Surg. 2001; 107:454–462. [PubMed: 11214061]
54. Wang J, Glimcher MJ. Characterization of matrix-induced osteogenesis in rat calvarial bone defects: IIOrigins of bone-forming cells. Calcif Tissue Int. 1999; 65:486–493. [PubMed: 10594169]
55. Wang J, Glimcher MJ. Characterization of matrix-induced osteogenesis in rat calvarial bone defects: I Differences in the cellular response to demineralized bone matrix implanted in calvarial defects and in subcutaneous sites. Calcif Tissue Int. 1999; 65:156–165. [PubMed: 10430651]
56. Gosain AK, Santoro TD, Song LS, et al. Osteogenesis in calvarial defects: Contribution of the dura, the pericranium, and the surrounding bone in adult versus infant animals. Plast Reconstr Surg. 2003; 112:515–527. [PubMed: 12900610]
57. Spector JA, Greenwald JA, Warren SM, et al. Dura mater biology: Autocrine and paracrine effects of fibroblast growth factor 2. Plast Reconstr Surg. 2002; 109:645–654. [PubMed: 11818848]
58. Opperman LA, Sweeney TM, Redmon J, et al. Tissue interactions with underlying dura mater inhibit osseous obliteration of developing cranial sutures. Dev Dyn. 1993; 198:312–322. [PubMed: 8130378]
59. Slater BJ, Kwan MD, Gupta DM, et al. Dissecting the influence of regional dura mater on cranial suture biology. Plast Reconstr Surg. 2008; 122:77–84. [PubMed: 18594389]
60. Kwan MD, Wan DC, Wang Z, et al. Microarray analysis of the role of regional dura mater in cranial suture fate. Plast Reconstr Surg. 2008; 122:389–399. [PubMed: 18626354]
61. Greenwald JA, Mehrara BJ, Spector JA, et al. Regional differentiation of cranial suture-associated dura mater in vivo and in vitro: Implications for suture fusion and patency. J Bone Miner Res. 2000; 15:2413–2430. [PubMed: 11127206]
62. Slater BJ, Kwan MD, Gupta DM, et al. The role of regional posterior frontal dura mater in the overlying suture morphology. Plast Reconstr Surg. 2009; 123:463–469. [PubMed: 19182602]
63. Roth DA, Bradley JP, Levine JP, et al. Studies in cranial suture biology: Part II Role of the dura in cranial suture fusion. Plast Reconstr Surg. 1996; 97:693–699. [PubMed: 8628762]
64. Yu JC, McClintock JS, Gannon F, et al. Regional differences of dura osteoinduction: Squamous dura induces osteogenesis, sutural dura induces chondrogenesis and osteogenesis. Plast Reconstr Surg. 1997; 100:23–31. [PubMed: 9207655]
65. Mehrara BJ, Most D, Chang J, et al. Basic fibroblast growth factor and transforming growth factor beta-1 expression in the developing dura mater correlates with calvarial bone formation. Plast Reconstr Surg. 1999; 104:435–444. [PubMed: 10654687]
66. Skillington J, Choy L, Derynck R. Bone morphogenetic protein and retinoic acid signaling cooperate to induce osteoblast differentiation of preadipocytes. J Cell Biol. 2002; 159:135–146. [PubMed: 12379805]

67. Wan DC, Shi YY, Nacamuli RP, et al. Osteogenic differentiation of mouse adipose-derived adult stromal cells requires retinoic acid and bone morphogenetic protein receptor type IB signaling. Proc Natl Acad Sci USA. 2006; 103:12335–12340. [PubMed: 16894153]

68. Mehlhorn AT, Niemeyer P, Kaschte K, et al. Differential effects of BMP-2 and TGF-beta1 on chondrogenic differentiation of adipose derived stem cells. Cell Prolif. 2007; 40:809–823. [PubMed: 18021172]

69. Knippenberg M, Helder MN, Zandieh Doulabi B, et al. Osteogenesis versus chondrogenesis by BMP-2 and BMP-7 in adipose stem cells. Biochem Biophys Res Commun. 2006; 342:902–908. [PubMed: 16500625]

70. Cabiling DS, Kim E, Yan D, et al. Differential effects of TGF-beta isoforms on murine fetal dural cells and calvarial osteoblasts. Plast Reconstr Surg. 2007; 120:614–624. [PubMed: 17700112]

71. Gosain AK, Recinos RF, Agresti M, et al. TGF-beta1, FGF-2, and receptor mRNA expression in suture mesenchyme and dura versus underlying brain in fusing and nonfusing mouse cranial sutures. Plast Reconstr Surg. 2004; 113:1675–1684. [PubMed: 15114129]

72. Opperman LA, Adab K, Gakunga PT. Transforming growth factor-beta 2 and TGF-beta 3 regulate fetal rat cranial suture morphogenesis by regulating rates of cell proliferation and apoptosis. Dev Dyn. 2000; 219:237–247. [PubMed: 11002343]

73. Roth DA, Longaker MT, McCarthy JG, et al. Studies in cranial suture biology: Part I Increased immunoreactivity for TGF-beta isoforms (beta 1, beta 2, and beta 3) during rat cranial suture fusion. J Bone Miner Res. 1997; 12:311–321. [PubMed: 9076573]

74. Opperman LA, Nolen AA, Ogle RC. TGF-beta 1, TGF-beta 2, and TGF-beta 3 exhibit distinct patterns of expression during cranial suture formation and obliteration in vivo and in vitro. J Bone Miner Res. 1997; 12:301–310. [PubMed: 9076572]

75. Bradley JP, Han VK, Roth DA, et al. Increased IGF-I and IGF-II mRNA and IGF-I peptide in fusing rat cranial sutures suggest evidence for a paracrine role of insulin-like growth factors in suture fusion. Plast Reconstr Surg. 1999; 104:129–138. [PubMed: 10597685]

76. Ferguson C, Alpern E, Miclau T, et al. Does adult fracture repair recapitulate embryonic skeletal formation? Mech Dev. 1999; 87:57–66. [PubMed: 10495271]

77. Gerstenfeld LC, Cho TJ, Kon T, et al. Impaired fracture healing in the absence of TNF-alpha signaling: The role of TNF-alpha in endochon-dral cartilage resorption. J Bone Miner Res. 2003; 18:1584–1592. [PubMed: 12968667]

78. Gupta DM, Kwan MD, Slater BJ, et al. Applications of an athymic nude mouse model of nonhealing critical-sized calvarial defects. J Craniofac Surg. 2008; 19:192–197. [PubMed: 18216688]

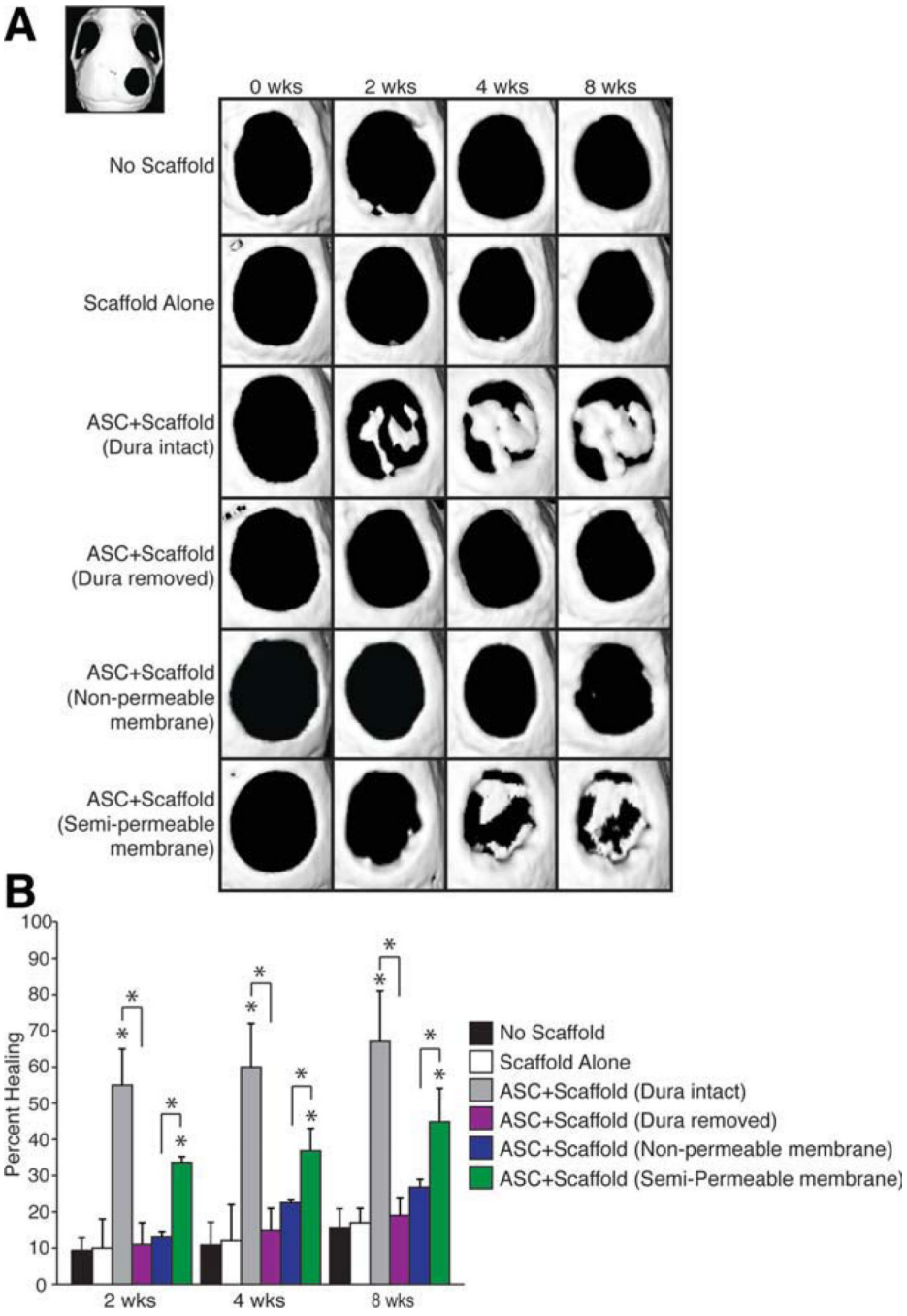

Figure 1.

Dura mater (DM) is required for human adipose-derived stromal cells (ASCs) to heal mouse calvarial defects. (**A**): Representative micro-X-ray computed tomography (micro-CT) images of defect sites at stratified time points postoperatively. The CT image in the upper left corner demonstrates the entire skull with the defect in the right parietal bone. Defects were either left empty, or treated with (a) no scaffold, (b) scaffold alone, (c) an hASC-engrafted scaffold with intact DM, (d) an hASC-engrafted scaffold with DM removed, (e) an hASC-engrafted scaffold with an impermeable silicone membrane placed between the

scaffold and intact, underlying DM, or (f) an hASC-engrafted scaffold with a semipermeable membrane placed between the scaffold and intact, underlying DM (n = 5 per group). (**B**): At 8 weeks, healing was quantified using Adobe Photoshop, expressed as average fraction osseous healing of the original defect size. A one-factor analysis of variance was used to compare the different treatment groups, followed by post hoc paired Student's t tests (with a Bonferroni correction) to assess significance. Asterisks placed directly over bars show significance when compared with control group (scaffold alone). Asterisks placed over bracket show significance between the groups indicated; *, $p < .05$. Abbreviation: ASC, adipose-derived stromal cell.

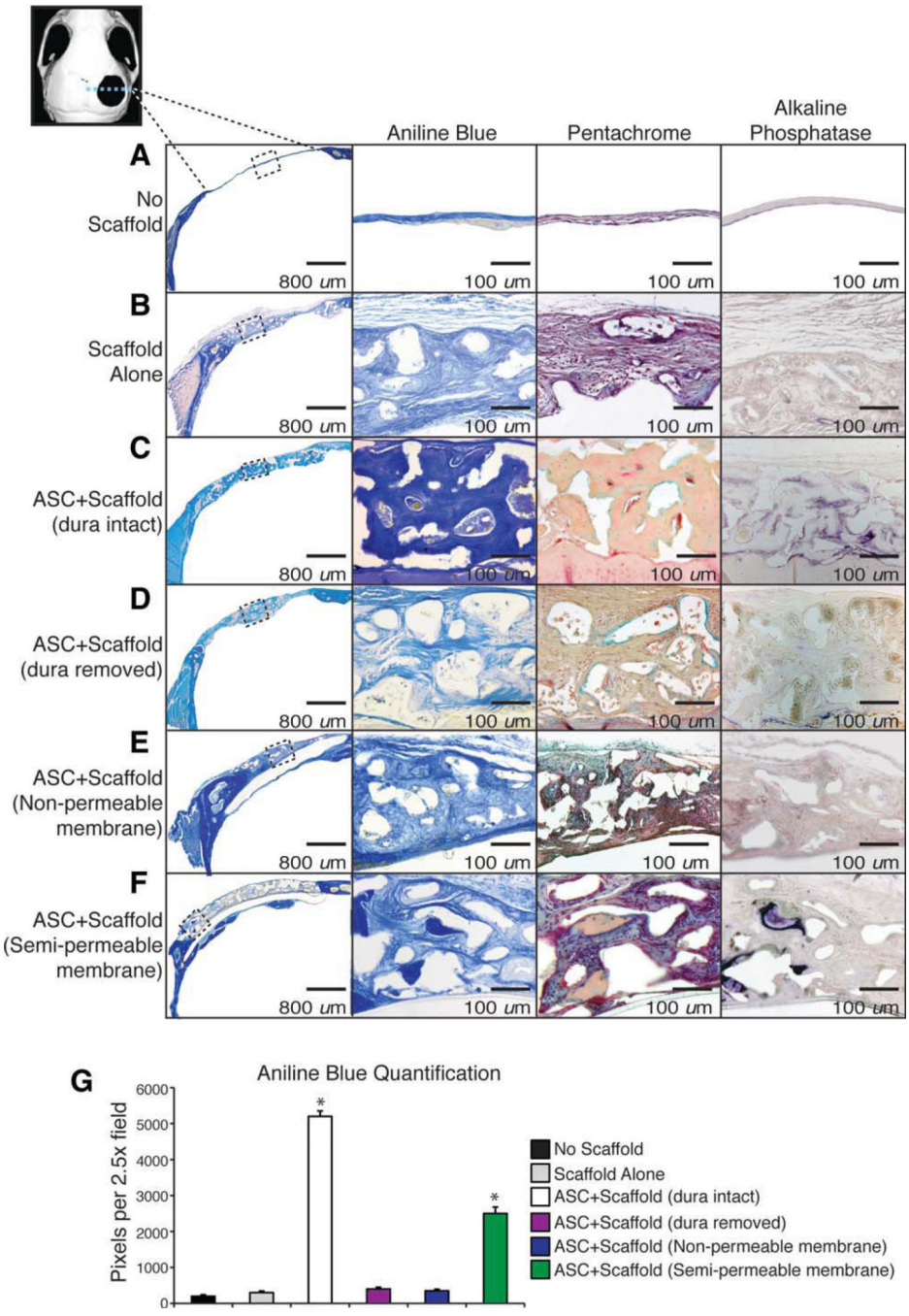

Figure 2.

Histologic analysis of bone formation. After 8 weeks, mice were sacrificed for histological analysis. Stains from left to right include: (a) low power aniline blue for orientation, (b) high power aniline blue to demonstrate osteoid, which is dark blue, (c) pentachrome stain, where mature osteoid is yellow, and (d) alkaline phosphatase, where activity is purple. Treatment groups include: (**A**) no scaffold, (**B**) scaffold alone (without human adipose-derived stromal cells [hASCs]), (**C**) hASC seeded scaffold with dura mater (DM) intact, (**D**) hASC seeded scaffold with disrupted DM, (**E**) hASC seeded scaffold with DM intact and a nonpermeable

membrane placed between the DM and overlying scaffold, and (**F**) hASC seeded scaffold DM intact and a semipermeable membrane placed between the underlying DM and overlying scaffold. (**G**): At 8 weeks, aniline blue positive bone per x2.5 field was quantified, $n = 50$ slides per group, five animals per group. A two-tailed Student's t test was performed to assess significance; *, $p < .05$. Boxes represent defect site at x20 magnification. Abbreviation: ASC, adipose-derived stromal cell.

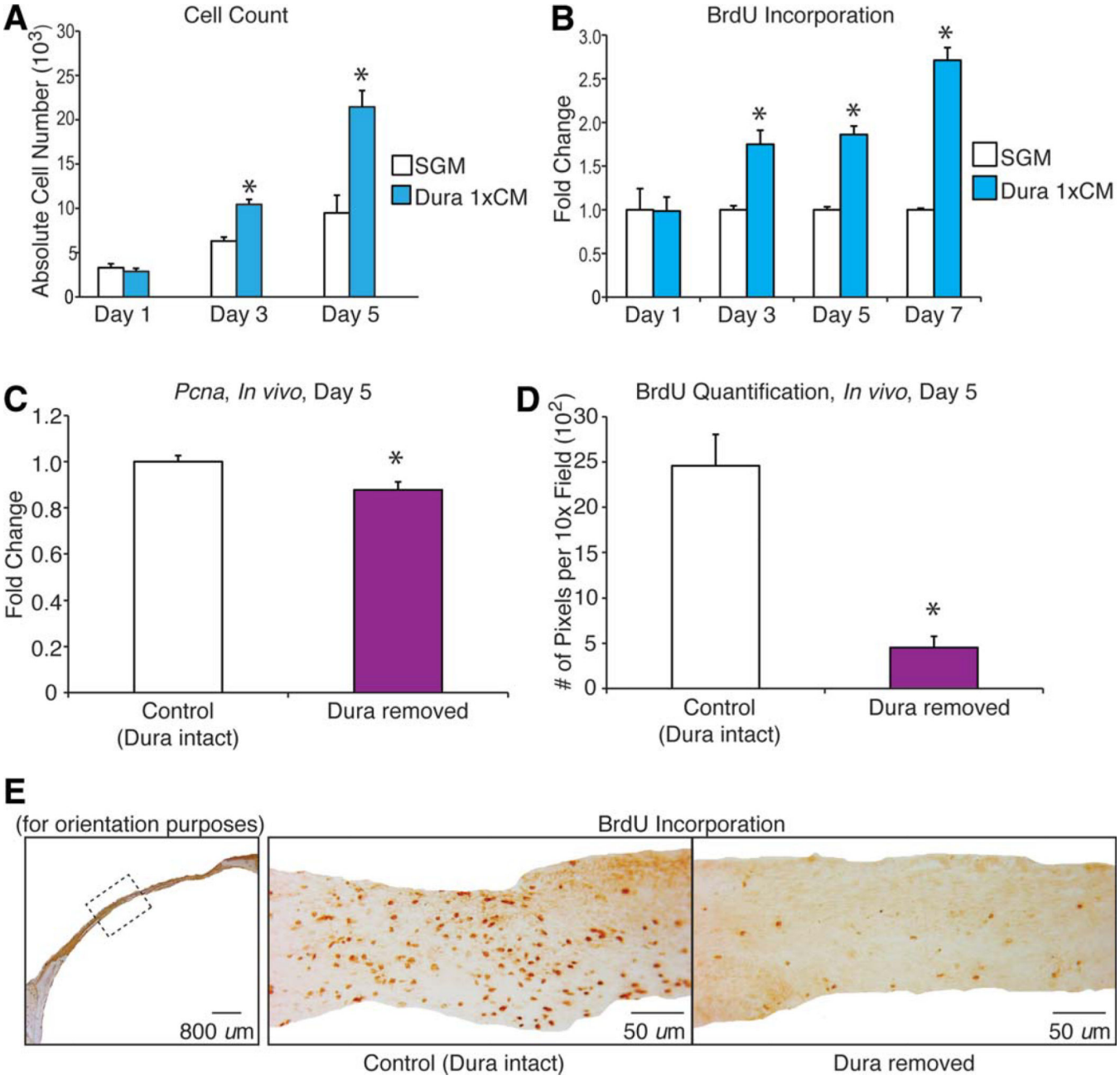

Figure 3.

Dura mater (DM) stimulates human adipose-derived stromal cell (hASC) proliferation in vitro and in vivo. (**A**): Cell counting assays of hASCs performed over 5 days in either standard growth medium (SGM) (Dulbecco's modified Eagle's medium, 10% FBS) or with SGM supplemented with DM conditioned media (CM). Cells were counted by trypsinization and hemocytometer analysis; *n* = 3 per group. (**B**): Bromodeoxyuridine (BrdU) incorporation assays of hASCs performed over 7 days of culture either in SGM or SGM supplemented with DM CM by enzyme-linked immunosorbent assay. Labeling reagent was applied for 8 hours in culture; *n* = 6 per group. (**C**): In vivo *Pcna* expression in calvarial defect tissue at postoperative day 5 in samples with intact or removed DM, *n* = 3. (**D**):

Quantification of BrdU immunostaining of calvarial defect at postoperative day 5 with intact or removed DM performed by Adobe Photoshop. 3,3′-Diaminobenzidine-positive bone per × 10 field was quantified, $n = 5$ slides per group, three animals per group. (**E**): BrdU immunostaining of calvarial defect tissue at postoperative day 5 with intact or removed DM. Hemicalvaria shown on left for orientation. Statistical significances were calculated between groups at individual days using a paired Student's *t* test; *, $p < .05$. Abbreviations: BrdU, bromodeoxyuridine; CM, conditioned media; SGM, standard growth medium.

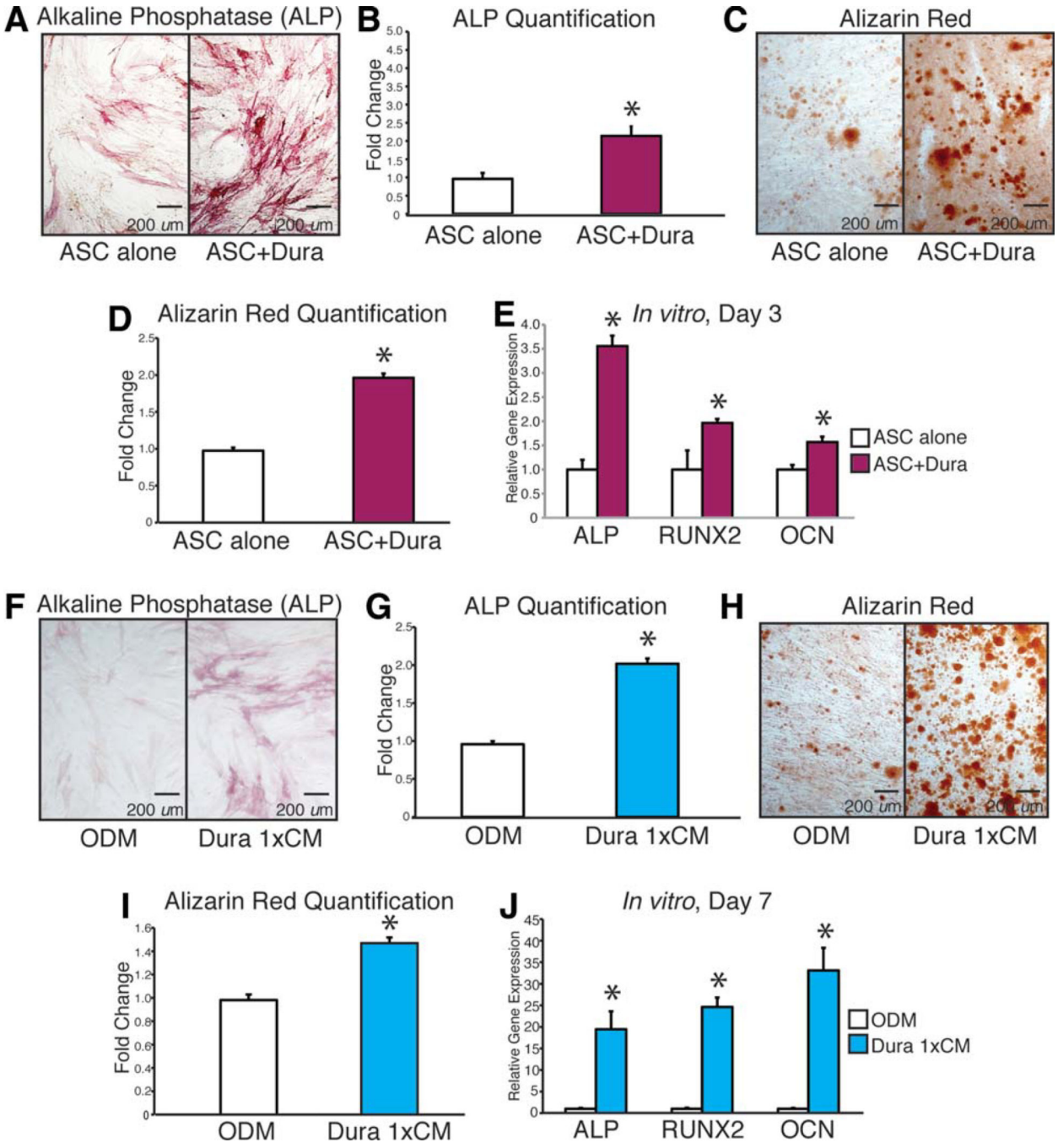

Figure 4.

Mouse dura mater (DM) cells stimulate human adipose-derived stromal cell (hASC) differentiation in vitro. (**A–E**): hASCs were cultured in osteogenic differentiation medium (ODM) in the presence or absence of mouse DM cells (noncontact coculture). (**A, B**): Alkaline phosphatase (ALP) stain and quantification of hASCs at 3 days differentiation. (**C, D**): Alizarin Red stain and quantification of hASCs at 7 days differentiation. (**E**): Gene expression profile of hASCs at 3 days differentiation grown in the presence or absence of mouse DM cells (noncontact coculture). Markers examined include osteogenic specific

genes: *ALP*, Runt-related protein-2 (*RUNX-2*), and osteocalcin (*OCN*). (**F–J**): Next, hASCs were cultured in ODM with or without the addition of mouse DM cell conditioned media (CM). (**F, G**): ALP stain and quantification of hASCs at 3 days differentiation. (**H, I**): Alizarin Red stain and quantification of hASCs at 7 days differentiation. (**J**): Gene expression profile of hASCs after 7 days differentiation in the presence or absence of DM cell CM. Markers examined include osteogenic specific genes *ALP*, *RUNX*-2, and *OCN* $n = 3$ for all assays (independent experiments from separately derived cell populations); *, $p < .05$. A two-tailed Student's *t* test was performed to assess significance. Abbreviations: ALP, alkaline phosphatase; ASC, adipose-derived stromal cell; CM, conditioned media; OCN, osteocalcin; ODM, osteogenic differentiation medium; RUNX-2, Runt-related protein-2.

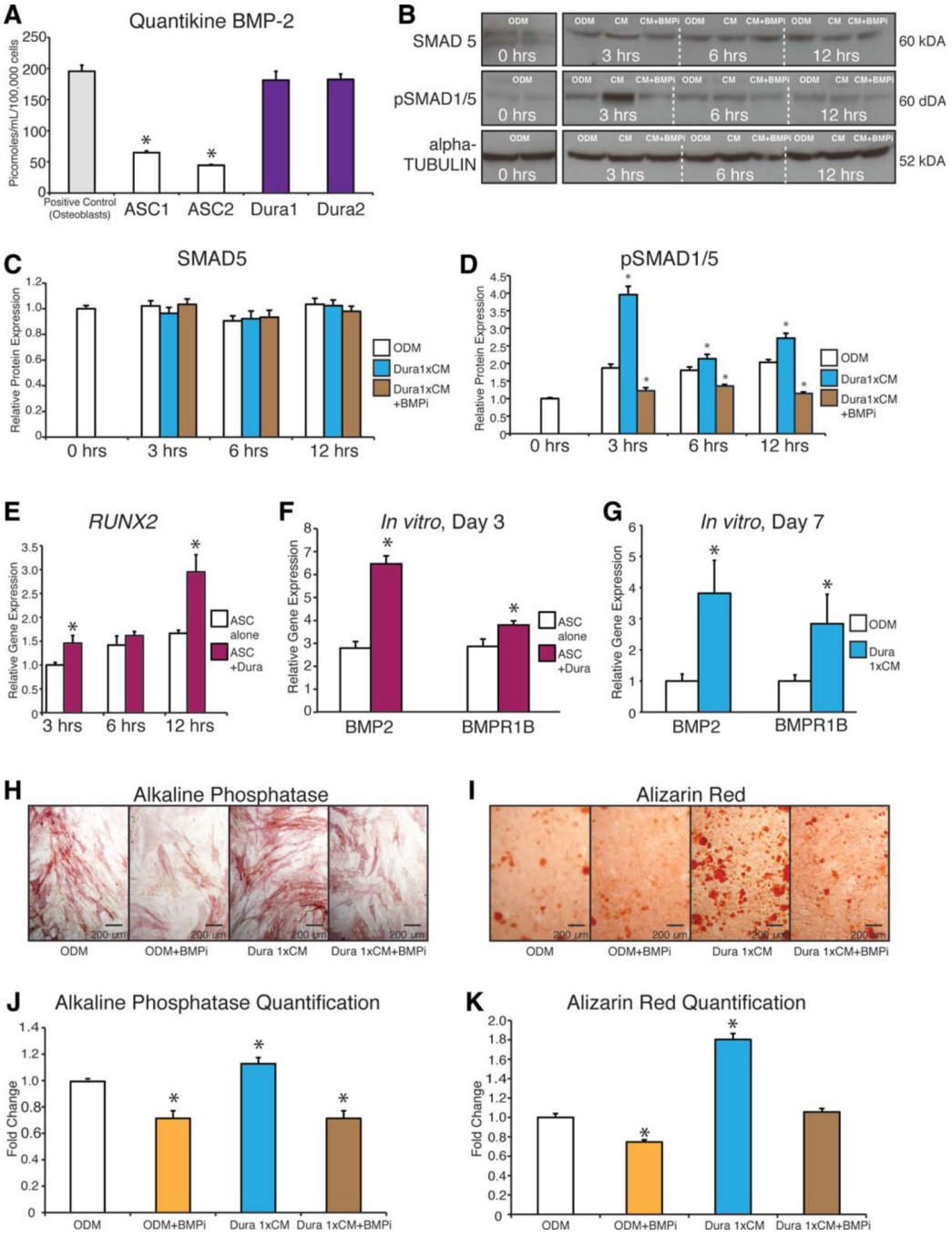

Figure 5.

Bone morphogenetic protein (BMP) signaling underlies the pro-osteogenic effect of the dura mater (DM)-human adipose-derived stro-mal cell (hASC) paracrine relationship. (**A**): Analysis of relative BMP-2 secretion, as assessed by BMP-2 enzyme-linked immunosorbent assay. Conditioned media (CM) was collected under serum-free conditions from mouse DM cells, hASCs, and mouse osteoblasts as a positive control. BMP-2 quantification (in picomoles) is based on known quantities of recombinant BMP-2, $n = 3$; *, $p < .05$. A two-tailed Student's *t* test was performed to assess significance. (**B**): Western blot image and

quantification of SMAD-5 and phosphorylated SMAD (pSMAD)-1/5 as well as alpha tubulin control for ASCs after exposure to osteogenic differentiation medium (ODM) alone, ODM with DM CM, or ODM with DM CM and a BMP-2/4 inhibitory antibody (BMPi) at 3, 6, and 12 hours. (**C**): Quantification of SMAD-5 protein at 0, 3, 6, and 12 hours after exposure to ODM, ODM plus DM CM, or CM or ODM with DM CM and a BMP-2/4 inhibitory antibody. (**D**): Quantification of active or pSMAD-1/5 protein at 0, 3, 6, and 12 hours after exposure to ODM, ODM plus DM CM, or CM or ODM with DM CM and a BMP-2/4 inhibitory antibody. (**E**) Expression of Runt-related protein-2 after 3, 6, and 12 hours of coculture of hASCs with DM cells by quantitative real-time polymerase chain reaction (qRT-PCR); *, $p < .05$. A two-tailed Student's *t* test was performed to assess significance, $n = 3$. (**F**): Expression of BMP-associated genes among hASCs with or without coculture with DM cells, by qRT-PCR; *, $p < .05$. A two-tailed Student's *t* test was performed to assess significance, $n = 3$. (**G**): Expression of BMP-associated genes among hASCs with or without supplementation with DM derived CM, by qRT-PCR; *, $p < .05$. A two-tailed Student's *t* test was performed to assess significance, $n = 3$. (**H–K**): Osteogenic differentiation assays of hASCs with or without DM CM and with or without neutralization by a anti-BMP-2/4 inhibitory antibody. (**H, J**): Alkaline phosphatase stain and quantification of hASCs under control conditions (ODM alone), ODM with BMPi, ODM with DM-derived CM, or ODM with DM CM and BMPi. (**I, K**): Alizarin Red stain and quantification of hASCs under control conditions (ODM alone), ODM with BMPi, ODM with DM-derived CM, or ODM with DM CM and BMPi, $n = 3$ for all assays; *, $p < .05$. A one-factor analysis of variance was used to compare different treatment groups, followed by a post hoc student's *t* test to assess significance. Abbreviations: ASC, adipose-derived stromal cell; BMP-2, bone morphogenetic protein-2; CM, conditioned media; ODM, osteogenic differentiation medium; pSMAD, phosphorylated SMAD; RUNX-2, Runt-related protein-2.

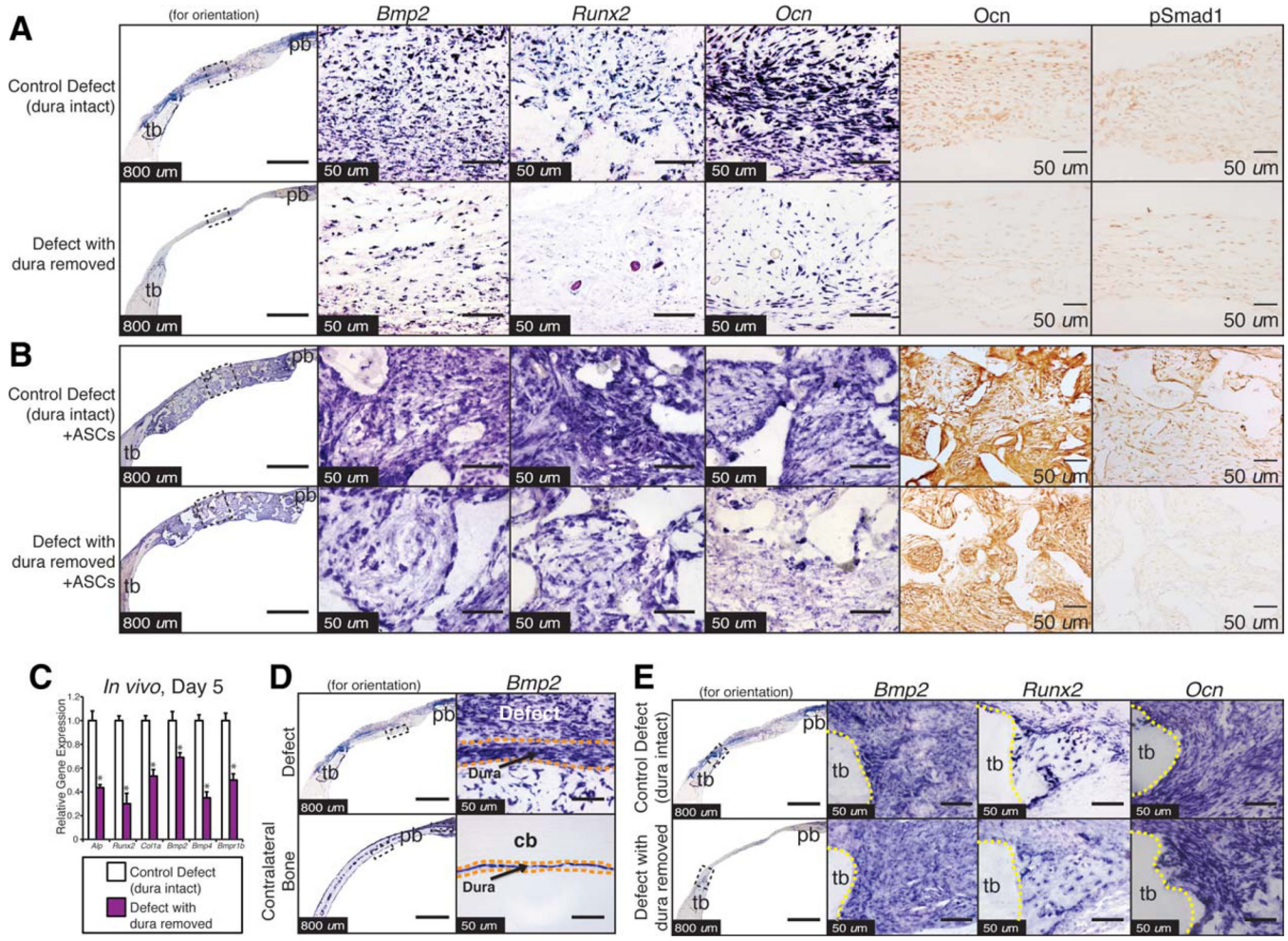

Figure 6.

Dura mater (DM) enhances bone morphogenetic protein (BMP) and osteogenic gene expression within mouse calvarial defects and on overlying human adipose-derived stromal cell (hASCs). (**A**): Histological analysis of the defect center postoperative day 5 with or without DM intact and without scaffolds or hASCs. On the left, an image of the defect site in the right parietal bone (pb) and surrounding calvaria is shown for orientation purposes. Second column: *Bmp-2* expression by in situ hybridization (ISH). Third column: Runt-related protein-2 (RUNX-2) expression by ISH. Fourth column: Osteocalcin (*Ocn*) expression by ISH. Immunohistochemistry analysis of Ocn (fifth column) and phosphorylated SMAD-1 (sixth column). Groups compared from top to bottom include (a) calvarial defect with the DM left intact and (b) calvarial defect with the DM removed. (**B**): Calvarial defect with the DM intact or removed and with a hASC seeded scaffold placed in the defect. Stains are the same as described in (**A**). (**C**): Quantitative real-time polymerase chain reaction analysis of RNA derived from cranial defects at 5-day postoperatively, specific for mouse genes. A significant reduction of *mAlp mRunx-2 mCol1a1 mBmp-2 mBmp-4*, and *mBmpr1b* was observed upon DM removal; $n = 5$ animals per group; *, $p < .05$. A paired Student's *t* test was performed to assess significance. (**D**): Histological analysis of the defect center postoperative day 5 with DM intact or with DM removed treated with a

scaffold with hASCs. On the left, an image of the defect site in the right pb and surrounding calvaria is shown for orientation purposes. Second column: *Bmp-2* expression by ISH specific for mouse. (**E**): Histological analysis of the defect edge postoperative day 5 with DM intact or with DM removed. On the left, an image of the defect site in the right pb and surrounding calvaria is shown for orientation purposes. Second column: *Bmp-2* expression by ISH. Third column: *Runx-2* expression by ISH. Fourth column: *Ocn* expression by ISH. Abbreviations: ASC, adipose-derived stromal cell; BMP-2, bone morphogenetic protein; cb, contralateral (uninjured) bone; OCN, osteocalcin; pb, parietal bone; pSMAD, phosphorylated SMAD; RUNX-2, Runt-related protein-2; tb, temporal bone.

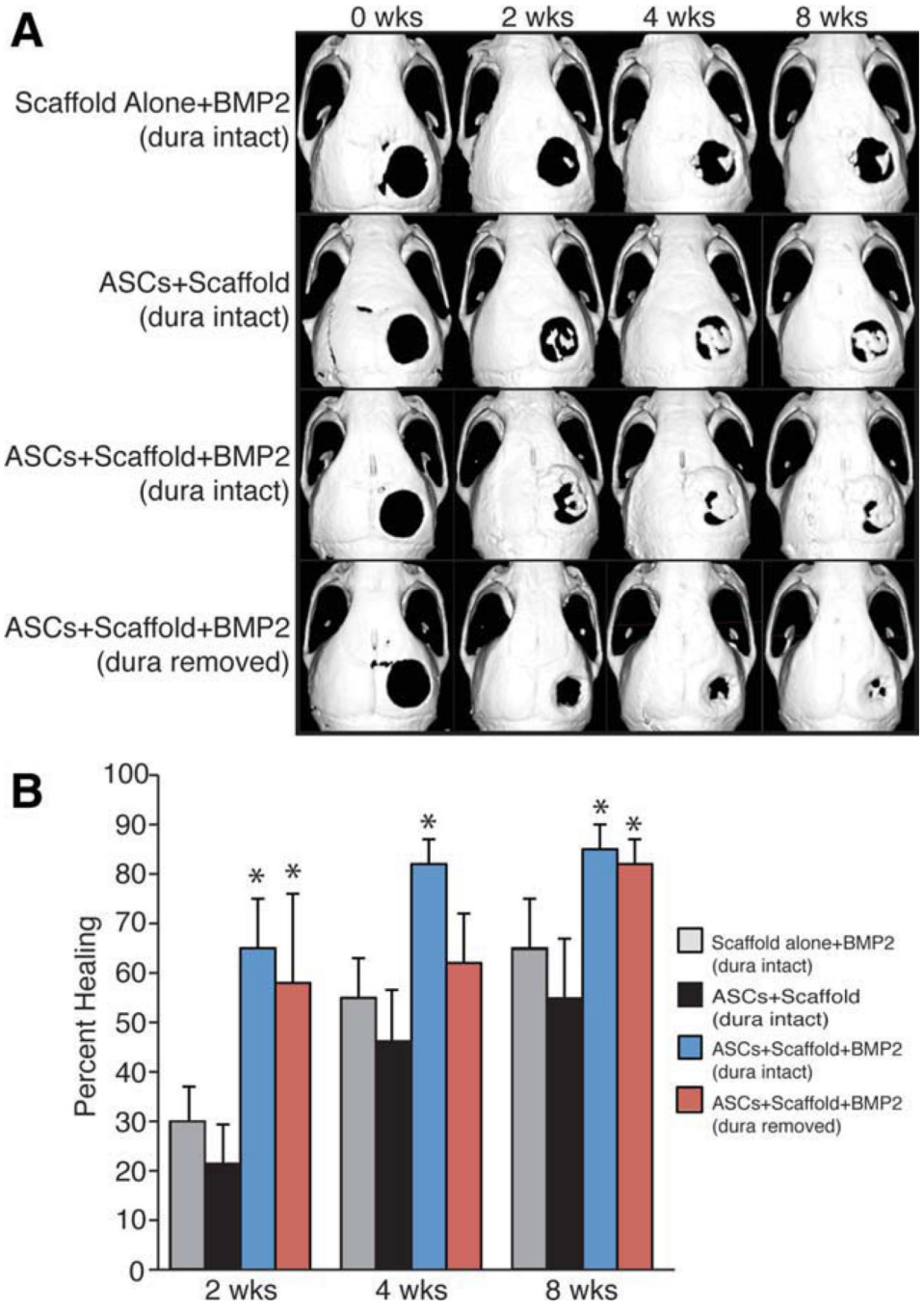

Figure 7.

Recombinant bone morphogenetic protein-2 (BMP-2) “rescues’ human adipose-derived stromal cell (hASC) mediated healing among defects with disrupted dura mater (DM)-hASC interaction. (**A**): Micro–X-ray computed tomography (micro-CT) CT images of defect sites at stratified time points postoperatively. DM was either left intact or removed at the defect site. Scaffolds were loaded with (200 μg) BMP-2 or phosphate-buffered saline control and engrafted with hASCs. From top to bottom, defects were treated with (a) a BMP-2 releasing scaffold with no hASCs (DM intact) for control purposes, (b) an hASC-engrafted scaffold

(DM intact), (c) an hASC-engrafted BMP-2 releasing scaffold (DM intact), or (d) an hASC-engrafted BMP-2 releasing scaffold following DM removal. (**B**): Healing was quantified by micro-CT and Adobe Photoshop analysis, expressed as average fraction osseous healing of the original defect size. A one-factor analysis of variance was used to compare the different treatment groups, followed by a post hoc student's *t* test to assess significance, $n = 3$; *, $p < .05$. Abbreviations: ASC, adipose-derived stromal cell; BMP-2, bone morphogenetic protein-2.